

# Sequential recombination algorithm for jet clustering and background subtraction

Jeff Tseng\* and Hannah Evans

*University of Oxford, Subdepartment of Particle Physics,  
Denys Wilkinson Building, Keble Road, Oxford OX1 3RH, United Kingdom*

(Dated: April 3, 2024)

We investigate a new sequential recombination algorithm which effectively subtracts background as it reconstructs the jet. We examine the new algorithm's behavior in light of existing algorithms, and we find that in Monte Carlo comparisons, the new algorithm's robustness against collision backgrounds is comparable to that of other jet algorithms when the latter have been augmented by further background subtraction techniques.

Collimated jets of particles are a distinctive feature of high energy elementary particle collisions and are often taken to indicate the presence of ejected quarks or gluons, particles normally shrouded by the effects of quantum chromodynamics (QCD). Jet reconstruction therefore plays a prominent role in event analysis, and as the search for new physics breaches new thresholds in energy and jet multiplicity, understanding jet reconstruction itself has taken on new importance. This importance is especially true in the study of highly relativistic (“boosted”) objects, in which evidence of heavy or exotic particle production and decay can be discerned in a jet's substructure. Experimental results on jet substructure have been published by the CDF [1], ATLAS [2, 3], and CMS [4] experiments.

A standard class of methods for jet reconstruction in hadron collider experiments is the sequential recombination algorithm. Different varieties of this algorithm usually are rooted in physical or geometric considerations, such as QCD splitting functions for the  $k_T$  algorithm [5, 6], angular ordering for Cambridge-Aachen [7], and collimated jet cores for anti- $k_T$  [8]. In this article, we consider a modified sequential recombination algorithm which has some features seen in the classical theory of radiation by moving charges. The algorithm simultaneously removes background radiation, including initial state radiation, particles of the underlying event, and those from the unassociated collisions (“pileup”) which are an important feature of modern high-luminosity colliders such as the Large Hadron Collider.

The first section of this article describes the modified algorithm and compares it with others. In Section II, we test the new algorithm on simulated high-energy  $W$  bosons with and without the presence of pileup, and compare the results with those of other clustering algorithms. Comparisons are also made with further background removal (“grooming”) techniques.

## I. ALGORITHM

In a typical sequential recombination algorithm, we start with a set of 4-vectors (“clusters”) which could represent the momenta of particles, calorimeter energy deposits, or previously clustered 4-vectors. The initial clusters are assumed to be massless. Interjet distances

$$d_{ij} = \min[p_{Ti}, p_{Tj}] \left( \frac{\Delta R_{ij}}{R} \right)^2 \quad (1)$$

are calculated for each pair of clusters  $i$  and  $j$ , as well as beam-jet distances

$$d_{iB} = p_{Ti} \quad (2)$$

for each cluster  $i$ . In these formulae,  $p_{Ti}$  is the momentum of cluster  $i$  transverse to the beam, and  $\Delta R_{ij} = \sqrt{(\Delta y_{ij})^2 + (\Delta \phi_{ij})^2}$ , where  $\Delta y_{ij}$  is the rapidity difference and  $\Delta \phi_{ij}$  the difference in azimuthal angle.  $R$  is a jet scale parameter which defines the maximum  $\Delta R_{ij}$  for clustering pairs. The parameter  $r$  is 2 for the  $k_T$  algorithm, 0 for Cambridge-Aachen, and  $-2$  for the anti- $k_T$  algorithm. If the smallest distance is a  $d_{ij}$ , the pair is merged, often by adding the 4-momenta. If the smallest distance is a  $d_{iB}$ , the cluster is deemed an independent jet and removed from further consideration. These steps are repeated until all clusters have been deemed jets.

We now consider a new algorithm with distance measures

$$d_{ij} = \frac{1}{4}(m_{Ti} + m_{Tj})^2 \left( \frac{\Delta R_{ij}}{R} \right)^3, \quad (3)$$

$$d_{iB} = m_{Ti}^2, \quad (4)$$

where  $m_{Ti} = \sqrt{m_i^2 + p_{Ti}^2}$  is the “transverse mass” of cluster  $i$ , and  $m_i$  is its mass.[9] The coefficient  $1/4$  has the effect that  $d_{iB} < d_{ij}$  whenever two jets with the same  $m_T$  are separated by  $\Delta R_{ij} > R$ . If  $m_{Ti} < m_{Tj}$ , we also have  $d_{iB} < d_{ij}$  whenever  $\Delta R_{ij} > R$ , and therefore  $R$  is, as in other algorithms, the maximum  $\Delta R_{ij}$  between clusters that can be merged. The algorithm is collinear and infrared-safe by construction. We call this algorithm “semi-classical” (SC) by analogy with the classical angular distribution of radiation from moving charges, which depends on the relativistic boost factor

---

\* j.tseng1@physics.ox.ac.uk

$\gamma \sim E_i + E_j \sim m_{T_i} + m_{T_j}$  (replacing energy by longitudinally invariant quantities), and has different exponents for the energy and angular ( $\Delta R_{ij}$ ) factors. The cubic angular exponent in Equation 3 arises from considering isotropic, massless emissions in the parent body's rest frame. Different exponents for the angular factor have been tested, and, for the most part, merely allow clusters to merge with larger or smaller  $\Delta R_{ij}$ , thus changing the size of the resulting jets.

The new energy factor, on the other hand, changes the way in which clusters are merged and set aside as jets, when compared with other algorithms. The  $k_T$  algorithm, for instance, starts by merging soft clusters, as one would expect for an algorithm which attempts to reverse the presumed history of  $1 \rightarrow 2$  splittings in the jet. At the same time, the  $k_T$  algorithm avoids the perceived problem of the JADE algorithm [10, 11], with distance measure

$$d_{ij} = E_i E_j (1 - \cos \theta_{ij}), \quad (5)$$

which can allow large angle clusterings of very soft pairs. The semi-classical algorithm also starts by merging soft pairs, though the raised  $\Delta R_{ij}$  exponent clusters some harder clusters sooner if they are sufficiently close. Large angle clusterings are suppressed by the  $R$  scale and beam clustering. However, the most significant difference in behavior between the semi-classical and  $k_T$  algorithms is that for sufficiently large  $\Delta R_{ij}$  (though still with  $\Delta R_{ij} < R$ ), the comparison with  $d_{iB}$  prevents a number of soft clusters from merging with high- $m_T$  clusters when

$$z'_{ij} \equiv \frac{m_{T_i}}{m_{T_i} + m_{T_j}} < \frac{1}{2} \left( \frac{\Delta R_{ij}}{R} \right)^{3/2}. \quad (6)$$

As a result, while  $R$  defines the maximum extent of a jet in the semi-classical algorithm, it is possible for two jets to be separated by  $\Delta R_{ij} < R$ . Moreover, the actual jets are likely to be narrower than  $R$ , with higher  $m_T$  associated with narrower jets. This behavior is similar to that of jet “pruning”, which vetoes mergings which satisfy the two conditions

$$z_{ij} \equiv \frac{\min(p_{T_i}, p_{T_j})}{|\vec{p}_{T_i} + \vec{p}_{T_j}|} < z_{cut}, \quad (7)$$

$$\Delta R_{ij} > D_{cut}, \quad (8)$$

and discards the softer of the two clusters [12, 13]. Figure 1 compares the two methods, with pruning removing the rectangular region in the  $(\Delta R_{ij}, z_{ij})$  plane, while the semi-classical algorithm additionally removes some soft clusters at small angles as well as harder clusters at large  $\Delta R_{ij}$ . These clusters become stand-alone jets separated by  $\Delta R_{ij} < R$ .

It is interesting to note that the area of a semi-classical jet, according to either the passive or active area definition of [15], is zero. This zero area is another reflection of the effect of the algorithm's “pruning” of background; from this perspective, further area-based back-

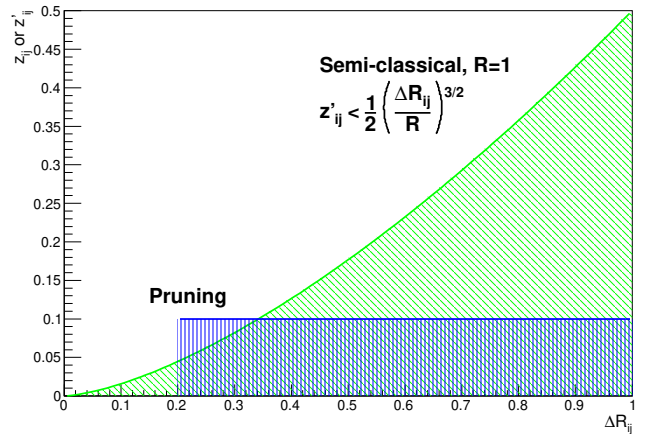


FIG. 1. Comparison of the semi-classical algorithm with pruning. The diagonally hashed region indicates mergings rejected by the semi-classical algorithm, while the vertically hashed region is for pruning. The pruning parameters are taken from [14].

ground subtraction is redundant. The effect of this pruning will be evident in the next Section's tests with simulated events.

## II. MONTE CARLO TESTS

Initial studies of the semi-classical algorithm with boosted objects have been performed using the PYTHIA (version 8.170) Monte Carlo generator [16, 17]. Single hadronically decaying  $W$ +parton events were generated with  $W$   $p_T > 500$  GeV/ $c$  at  $\sqrt{s} = 8$  TeV. Non-neutrino particles were then collected into  $0.1 \times 0.1$   $\eta - \phi$  cells out to  $|\eta| < 5$ , where  $\eta = -\ln[\tan(\theta/2)]$  is pseudorapidity. Up to an average of 25 QCD minimum bias events, using Tune 4Cx [18] and the CTEQ6L1 parton distribution functions [19], were overlaid as “pileup”, assuming the same interaction vertex. Only cells with energy greater than 0.5 GeV were considered for jet clustering. Jets were then found using the  $k_T$ , Cambridge-Aachen, and anti- $k_T$  algorithms implemented in FASTJET version 3.0.4 [20]. The semi-classical algorithm was implemented as a FASTJET plugin SCJET [21] version 1.1.0. Jet masses were calculated by summing the 4-momenta of the cells, assuming zero mass for each cell.

Figure 2(a) shows the jet mass distribution for jets with  $p_T > 400$  GeV/ $c$  in the same hemisphere as the generated  $W$  for different ungroomed jet algorithms with  $R = 1$ . Even with no pileup, the effect of additional radiation can be seen in the other algorithms, while the semi-classical peak is narrowest and lies closest, at  $80.9 \pm 0.1$  GeV/ $c^2$ , to the generated  $W$  mass of 80.385 GeV/ $c^2$ . The low and zero-mass bumps are the result of the semi-classical algorithm “pruning” close but energetically unbalanced  $W$  daughters, as noted above; combining the jet with another nearby jet recovers the  $W$  mass. When the pileup

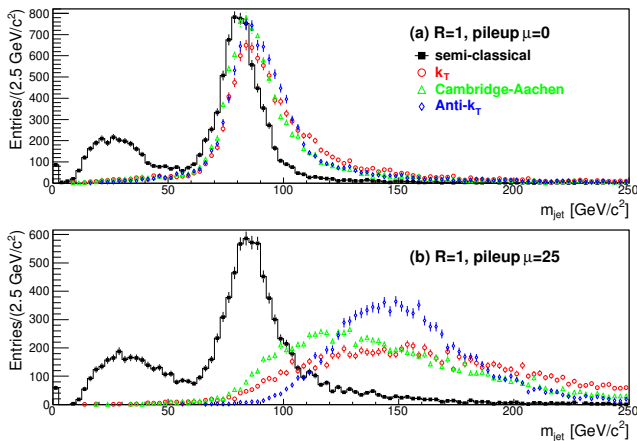


FIG. 2. Jet mass distributions for high- $p_T$  jets in the same hemisphere as the generated  $W$  boson, with an average of 25 pileup events overlaid and  $R = 1$  for the semi-classical,  $k_T$ , Cambridge-Aachen, and anti- $k_T$  algorithms: (a) no pileup; (b) with an average of 25 pileup events overlaid.

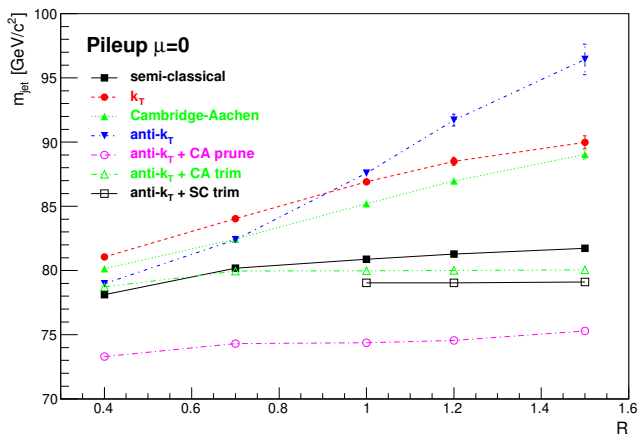


FIG. 3. Peak mass vs  $R$  for events with zero pileup.

level increases to an average of 25, as shown in Figure 2(b), the semi-classical peak shifts roughly  $4 \text{ GeV}/c^2$  higher, but remains a recognizable, narrow peak, while the others are much broader due to incorporating pileup radiation.

The effects of additional radiation usually are mitigated by reducing the  $R$  parameter, and indeed one can see in Figure 3 that at  $R = 0.4$ , all the peak masses cluster around  $80 \text{ GeV}/c^2$ , rising rapidly for the other ungroomed algorithms. The semi-classical algorithm, on the other hand, starts low at  $R = 0.4$ , where the two  $W$  daughters often are resolved into different jets, and levels off above  $R = 0.7$ .

Boosted object analyses, however, typically use large  $R$  values between 1 and 1.5 in order to remain sensitive to a larger range of energies. In order to mitigate pileup effects in such large jets, the jet can undergo further “grooming”. It is therefore instructive to compare

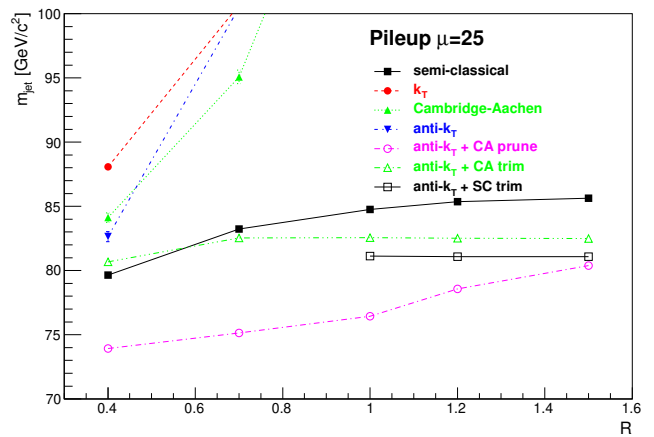


FIG. 4. Peak mass vs  $R$  for events with average 25 pileup. For most values of  $R$  for the  $k_T$ , Cambridge-Aachen, and anti- $k_T$  algorithms, the distributions are broad rather than peaked.

the new algorithm with grooming techniques, several of which, including pruning, are also shown in Figures 3 and 4. It should be noted that grooming techniques usually are tailored to particular environments, and rely on knowledge of the target final state such as one might use to design a search strategy based on individually resolved jets. The comparisons shown in this article are therefore indicative, leaving optimization for specific signals and backgrounds for those particular analyses.

Pruning has already been described. We start with anti- $k_T$  jets with a given  $R$ , and use the parameters  $z_{cut} = 0.1$  and  $D_{cut} = 0.2$  [14] to prune. We compare the resulting jets with those from the semi-classical algorithm by itself, with the same  $R$ . Not surprisingly, the two algorithms behave similarly in Figures 3 and 4, even rising at a similar rate as the average pileup level increases to 25. Jet mass distributions for  $R = 1.5$  are shown in Figure 5(a). The presence of pileup shifts the peaks of the distributions upward, as expected. The semi-classical algorithm, however, leaves a larger high-mass tail, but also a smaller low-mass bump, suggesting that while it eliminates less pileup radiation, it retains the  $W$  daughters more often. It is also evident that the given pruning parameters are too aggressive for these particular conditions, resulting in a low peak mass.

Next, we consider the grooming technique of trimming, which attempts to discern narrow, high- $p_T$  subjects within the parent jet [22, 23]. For the comparison, we use the Cambridge-Aachen algorithm to recluster within the parent jet with a smaller radius parameter  $R_{sub} = 0.3$ , and discard the resulting subjects with  $p_T < f_{sub} P_T$ , where  $f_{sub} = 0.05$  is a parameter and  $P_T$  is the transverse momentum of the parent jet [14]. The jet mass is then calculated by summing the remaining high- $p_T$  subjects. Figure 4 shows trimming to be more stable under these pileup conditions than pruning or the ungroomed semi-classical algorithm.

The semi-classical algorithm can be used for reclus-

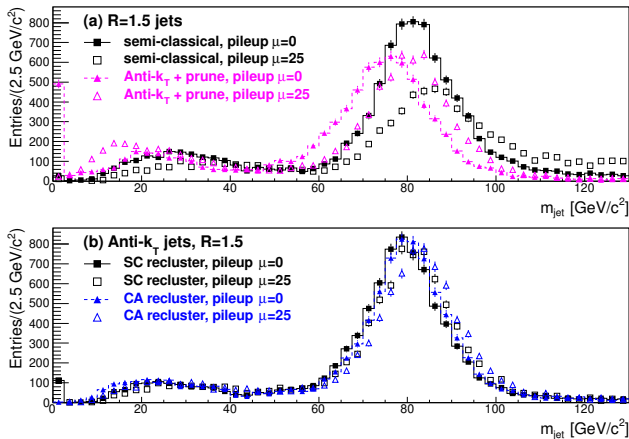


FIG. 5. (a) Jet mass distributions for high- $p_T$  semi-classical and pruned anti- $k_T$  jets in the same hemisphere as the generated  $W$  boson, with zero and average 25 pileup. (b) Trimmed jet mass distributions, reclustered by the Cambridge-Aachen ( $R_{sub} = 0.3$ ) and semi-classical ( $R_{sub} = 0.4$ ) algorithms, with zero and average 25 pileup.

tering; in effect, such a method combines pruning and conventional trimming. We use a slightly larger value of  $R_{sub} = 0.4$  to compensate for the smaller semi-classical jets, and we trim anti- $k_T$  jets with  $R \geq 1$ . Figure 5(b) shows the results of reclustering with the Cambridge-Aachen and semi-classical algorithms. As may be expected, the mass distributions are very similar, again with low-mass bumps where another  $W$  daughter has been discarded by the trimming technique. The distributions are largely insensitive to both the parent jet's  $R$  parameter, as also shown in Figures 3 and 4, as well as to the pileup level.

Figures 6 and 7 compare the effects of increasing the pileup level on the different ungroomed and groomed algorithms for large  $R$  values. The difference between ungroomed and groomed jets is more obvious here, with the mass peak rapidly rising and broadening at even modest levels of pileup for all the ungroomed algorithms except the semi-classical algorithm. The ungroomed semi-classical algorithm parallels pruning over this range of pileup level, while the peak  $W$  masses of trimming, with either reclustering algorithm, rises more slowly than those for pruning.

### III. CONCLUSION

In this article, we have investigated the behavior of a sequential recombination algorithm with a new inter-cluster distance measure  $d_{ij}$  which depends on the sum of clusters' transverse masses. The resulting algorithm effectively combines jet clustering with pruning-like behavior in one step. Monte Carlo tests with PYTHIA8 show the algorithm by itself performing like an algorithm with jet grooming in terms of stability with respect to the jet

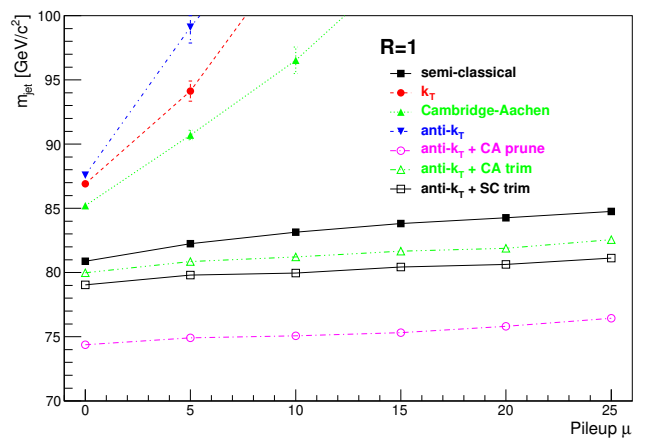


FIG. 6. Dependence of mass peak position on pileup for different algorithms with  $R = 1$ . The mass distributions at most or all pileup levels for the  $k_T$ , Cambridge-Aachen, and anti- $k_T$  algorithms are very broad, with maxima above  $100 \text{ GeV}/c^2$ .

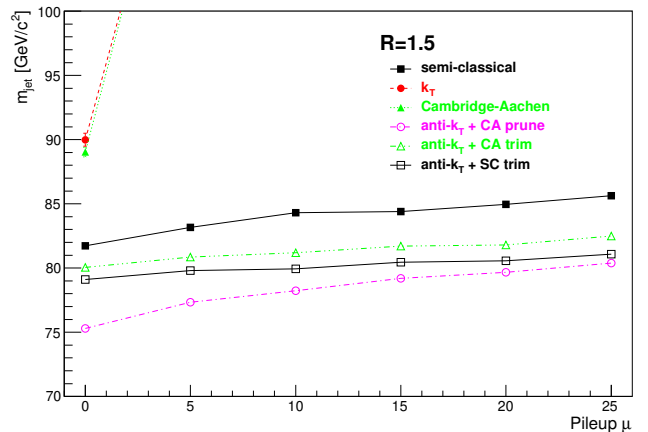


FIG. 7. Dependence of mass peak position on pileup for different algorithms with  $R = 1.5$ . The mass distributions at most or all pileup levels for the  $k_T$ , Cambridge-Aachen, and anti- $k_T$  algorithms are very broad, with maxima above  $100 \text{ GeV}/c^2$ . The anti- $k_T$  mass distribution peaks near  $100 \text{ GeV}/c^2$  even at zero pileup.

scale parameter  $R$  as well as to pileup. It can also be used to recluster narrow subjets for trimming. Further work would be needed to determine whether cross sections can be calculated for the new algorithm without large QCD corrections. At the same time, as has been observed widely (and wisely), Monte Carlo studies may show the feasibility of a method, but they are a far cry from optimizing and testing it in a genuine experimental context.

### ACKNOWLEDGMENTS

This work was supported by the Science and Technology Facilities Council of the United Kingdom and the

Higher Education Funding Council of England. The authors would like to thank A Cooper-Sarkar, C Issever,

BT Huffman, and G Salam for useful comments and discussion.

- 
- [1] T. Aaltonen *et al.* (CDF Collaboration), Phys.Rev., **D85**, 091101 (2012), arXiv:1106.5952 [hep-ex].
  - [2] G. Aad *et al.* (ATLAS Collaboration), JHEP, **1205**, 128 (2012), arXiv:1203.4606 [hep-ex].
  - [3] G. Aad *et al.* (ATLAS Collaboration), (2013), arXiv:1306.4945 [hep-ex].
  - [4] S. Chatrchyan *et al.* (CMS Collaboration), (2013), arXiv:1303.4811 [hep-ex].
  - [5] S. Catani, Y. L. Dokshitzer, M. Seymour, and B. Webber, Nucl.Phys., **B406**, 187 (1993).
  - [6] S. D. Ellis and D. E. Soper, Phys.Rev., **D48**, 3160 (1993), arXiv:hep-ph/9305266 [hep-ph].
  - [7] M. Wobisch and T. Wengler, (1998), arXiv:hep-ph/9907280 [hep-ph].
  - [8] M. Cacciari, G. P. Salam, and G. Soyez, JHEP, **0804**, 063 (2008), arXiv:0802.1189 [hep-ph].
  - [9] An earlier version of the algorithm used  $E_T$ , the transverse energy, instead of  $m_T$ , which has the advantage of being longitudinally invariant. The differences are small for the tests presented in this article.
  - [10] W. Bartel *et al.* (JADE Collaboration), Z.Phys., **C33**, 23 (1986).
  - [11] S. Bethke *et al.* (JADE Collaboration), Phys.Lett., **B213**, 235 (1988).
  - [12] S. D. Ellis, C. K. Vermilion, and J. R. Walsh, Phys.Rev., **D80**, 051501 (2009), arXiv:0903.5081 [hep-ph].
  - [13] S. D. Ellis, C. K. Vermilion, and J. R. Walsh, Phys.Rev., **D81**, 094023 (2010), arXiv:0912.0033 [hep-ph].
  - [14] ATLAS Collaboration, ATLAS-CONF-2012-066, ATLAS-COM-CONF-2012-097 (2012).
  - [15] M. Cacciari, G. P. Salam, and G. Soyez, JHEP, **0804**, 005 (2008), arXiv:0802.1188 [hep-ph].
  - [16] T. Sjostrand, S. Mrenna, and P. Z. Skands, JHEP, **0605**, 026 (2006), arXiv:hep-ph/0603175 [hep-ph].
  - [17] T. Sjostrand, S. Mrenna, and P. Z. Skands, Comput.Phys.Commun., **178**, 852 (2008), arXiv:0710.3820 [hep-ph].
  - [18] R. Corke and T. Sjostrand, JHEP, **1105**, 009 (2011), arXiv:1101.5953 [hep-ph].
  - [19] J. Pumplin, D. Stump, J. Huston, H. Lai, P. M. Nadolsky, *et al.*, JHEP, **0207**, 012 (2002), arXiv:hep-ph/0201195 [hep-ph].
  - [20] M. Cacciari and G. P. Salam, Phys.Lett., **B641**, 57 (2006), arXiv:hep-ph/0512210 [hep-ph].
  - [21] <http://www-pnp.physics.ox.ac.uk/~tseng/scplugin/> and <http://fastjet.hepforge.org/contrib/>.
  - [22] D. Krohn, J. Thaler, and L.-T. Wang, JHEP, **1002**, 084 (2010), arXiv:0912.1342 [hep-ph].
  - [23] A. Abdesselam, E. B. Kuutmann, U. Bitenc, G. Brooijmans, J. Butterworth, *et al.*, Eur.Phys.J., **C71**, 1661 (2011), arXiv:1012.5412 [hep-ph].